Antiferromagnetic Alkali Metal Oxohydroxoferrates(III) with Correlated Hydrogen Bonding Systems

Ralf Albrecht,[a] Jens Hunger,[a] Markus Hölzel,[b] Theresa Block,[c] Rainer Pöttgen,[c] Thomas Doert,[a] and Michael Ruck*[a, d]

Dedicated to Professor Arndt Simon on the Occasion of his 80th Birthday

The oxohydroxoferrates(III) $A_2[Fe_2O_3(OH)_2]$ ($A = $ K, Rb, Cs) were synthesized under hydroflux conditions. Approximately equimolar mixtures of the alkali metal hydroxides and water were reacted with $Fe(NO_3)_3 \cdot 9H_2O$ at about 200 °C. The product formation depends on the hydroxide concentration, therefore also other reaction products, such as $KFeO_2$, $K_{2-x}[Fe_4O_{7-x}(OH)_x]$ or α-Fe_2O_3, are obtained. The crystal structures of the oxohydroxoferrates(III) $A_2[Fe_2O_3(OH)_2]$ follow the same structural principle, yet differ in their layer stacking or/and their hydrogen bonding systems depending on A and temperature. In the resulting four different orthorhombic structure types, $[FeO_3OH]^{4-}$ tetrahedra share their oxide corners to create folded $_\infty^2[Fe_2O_3(OH)_2]^{2-}$ layers. The terminal hydroxide ligands form hydrogen bonds between and/or within the layers. The positions of the hydrogen atoms in these networks are correlated. The A^+ cations are located between the folded anionic layers as well as in their trenches. Under reaction conditions, the potassium compound crystallizes in the space group $Cmce$ (Pearson symbol $oC88$), showing a bimodal disorder of the hydrogen atoms in hydrogen bridges. In a virtually hysteresis-less first-order transition at 340(2) K, the structure slightly distorts into the room-temperature modification with the subgroup $Pbca$ ($oP88$), and the hydrogen atoms order. The rubidium and caesium compounds are isostructural to each other but not to the potassium compound, and are always obtained as mixtures of two modifications with space groups $Cmce$ ($oC88'$) and $Immb$ ($oI88$). Upon heating, the oxohydroxoferrates decompose into their anhydrides $AFeO_2$ and water. The type of hydrogen bonding network influences the decomposition temperature, the structure and the morphology of the crystals. Despite the presence of iron(III), which was confirmed by ^{57}Fe-Mössbauer spectroscopy, $K_2[Fe_2O_3(OH)_2]$ is diamagnetic in the investigated temperature range between 1.8 and 300 K. Neutron diffraction revealed strong antiferromagnetic coupling of the magnetic moments, which are inverted in neighboring tetrahedra.

1. Introduction

Oxohydroxoferrates may be regarded as hydrated forms of water-free oxoferrates. While a broad variety of alkali metal oxoferrates(III) was described, such as $AFeO_2$ ($A = $ K, Rb, Cs),[1] $A_4Fe_2O_5$ ($A = $ Na, K),[2] $K_{14}Fe_4O_{13}$,[3] $K_{17}Fe_5O_{16}$[4] or $K_6Fe_2O_6$,[5] quaternary alkali metal oxohydroxoferrates(III) were up to now unknown. The oxoferrate(II) hydroxide $Na_5[FeO_3]OH$ contains iron(II) in trigonal $[FeO_3]^{4-}$ units and "isolated" hydroxide ions.[6] With alkaline earth metals, the oxoferrate(II,III) hydroxoferrate (III) $Ba_4[Fe_8O_{14}][Fe(OH)_6]$[7] and the perovskite $Ba[FeO_{2.5-x}(OH)_{2x}]$,[8] were described. Highly remarkable is the mixed-metal oxoferrate(III) hydroxide $Ba_8(Fe_{12}O_{24})Na_y(OH)_6 \cdot xH_2O$,[9] which is a zeolitic framework of iron-centered tetrahedra hosting hydroxide ions and counter cations in its channels.

We now present three new oxohydroxoferrates with the formula $A_2[Fe_2O_3(OH)_2]$ ($A = $ K, Rb, Cs). Beside their hydroflux synthesis we report their crystal structures, their chemical and thermal decomposition as well as their magnetic properties. The three compounds are abbreviated as ***K*** for $K_2[Fe_2O_3(OH)_2]$, ***Rb*** and ***Cs*** for the corresponding rubidium and caesium compounds.

The hydroflux method,[10] which we employed here, is based on a highly concentrated mixture of alkali metal hydroxide (AOH) and water as reaction medium. Typically, the molar ratio $q(A) = n(AOH):n(H_2O)$ is close to one. The properties of such a medium resemble a pure hydroxide flux, as a strong basic character and high solubility for oxidic compounds are given. Adding small amounts of water lowers successively the melting point of the alkali-metal hydroxide (neat KOH: $T_m = 360$ °C; $KOH \cdot H_2O$: $T_m = 143$ °C). Upon adding larger quantities of water, the domain of hydrothermal conditions is reached.

[a] R. Albrecht, Dr. J. Hunger, Prof. Dr. T. Doert, Prof. Dr. M. Ruck
Faculty of Chemistry and Food Chemistry
Technische Universität Dresden, 01069 Dresden (Germany)
E-mail: michael.ruck@tu-dresden.de
Homepage: https://tu-dresden.de/mn/chemie/ac/ac2/
[b] Dr. M. Hölzel
Forschungsneutronenquelle Heinz Maier-Leibnitz (FRM II), Technische Universität München
Lichtenbergstraße 1, 85747 Garching (Germany)
[c] T. Block, Prof. Dr. R. Pöttgen
Institut für Anorganische und Analytische Chemie, Universität Münster, Corrensstraße 30, 48149 Münster, Germany
[d] Prof. Dr. M. Ruck
Max-Planck Institute for Chemical Physics of Solids
Nöthnitzer Straße 40, 01187 Dresden (Germany)

2. Results and Discussion

2.1. Synthesis

Greenish-yellow crystals of the oxohydroxoferrates (yield $>99\%$) were obtained as plates of various shapes by reacting iron(III) nitrate nonahydrate with a mixture of the respective alkali metal hydroxide and water (q(K) = 1.1 and q(Rb/Cs) = 0.7) in a PTFE-lined stainless steel autoclave. The use of a closed autoclave with a PTFE inlet is required due to the corrosivity of the medium and the necessary constant base concentration, although almost no pressure is generated during the reaction.[10] After the synthesis all products were washed with dry methanol and stored under argon due to their instability against moisture. In air, the crystals of the oxohydroxoferrates quickly decompose to a red powder of an amorphous iron oxo-compound.

The base concentration q(A) of the hydroflux turned out to be the most important factor for the synthesis of the oxohydroxoferrates. With KOH, four phases were found in different concentration ranges: α-Fe$_2$O$_3$, K$_{2-x}$[Fe$_4$O$_{7-x}$(OH)$_x$],[11] **K**, and KFeO$_2$ (Figure 1). q(K) $\leq$ 0.5 results in phase pure α-Fe$_2$O$_3$ in the form of dark-red hexagonal crystals (Figure S1, Supporting Information). With increasing base concentrations, red hexagonal plates of K$_{2-x}$[Fe$_4$O$_{7-x}$(OH)$_x$] form in addition and their relative amount grows until phase-pure K$_{2-x}$[Fe$_4$O$_{7-x}$(OH)$_x$] is obtained at q(K) = 0.7 (Figures S2 and S3, Supporting Information). At q(K) = 0.9, few crystals of **K** appear besides K$_{2-x}$[Fe$_4$O$_{7-x}$(OH)$_x$], at q(K) = 1.1, phase-pure synthesis of **K** is achieved (Figure S4 and S5, Supporting Information). Above this concentration, KFeO$_2$, the anhydride of **K**, starts to form as ochre green distorted octahedra, and exceeding q(K) = 1.4, this is the only product (Figure S6 and S7, Supporting Information). No other product was found up to the highest tested q(K) of 1.8. To conclude, with increasing KOH concentration, the K to Fe ratio in the products increases until the hygroscopic nature of the hydroflux leads to the formation of an anhydride with n(K):n(Fe) = 1. Extreme base concentrations have no significant influence on the hydroflux reactions, but affect the melting point of the hydroflux, making the syntheses impractical. Up to now, the only other concentration dependent product formation in hydroflux reactions was reported for copper, where compounds with copper in different oxidations states were obtained.[12]

The synthesis temperature seems to have minor impact on the formation of phase-pure products, but at temperatures far below the optimum of 200 °C, a drastically shrinking of the average crystal size was observed. Cooling rates of -5 K/h and reaction times of at least 2 d provided single-crystals of **K** larger than 0.4 mm (Figure 2), although completely crystalline products can be received with holding times lower than 10 h. Significantly larger platelets of **K** (>1 mm edge length) were found in reactions with lower base concentration, where, however, K$_{2-x}$[Fe$_4$O$_{7-x}$(OH)$_x$] is the main product (see above).

With RbOH or CsOH, α-Fe$_2$O$_3$, is obtained at q(A) = n(AOH):n(H$_2$O) $<$ 0.5. The synthesis of **Rb** and **Cs** results in pure products, both in the form of two orthorhombic polymorphs that are visually distinguishable: square plates with the space group *Cmce* (Pearson symbol *oC*88′) and triangular capped bars with the space group *Immb* (*oI*88). The ratios of the polymorphs in the samples of **Rb** and **Cs** were rather similar, approximately 3:1 (Figure S8 and S9, Supporting Information). We were not able to obtain only one of the modifications by varying the reaction temperature or the base concentration (Figure S10, Supporting Information). In contrast, **K**(*oP*88) forms plates with a high variety of shapes for both modifications.

EDX measurements confirm the compositions A_2[Fe$_2$O$_3$(OH)$_2$] within the limits of the method (Table S1, Supporting Information). The slightly lower alkali metal content might be a result of the washing process with methanol under ambient conditions and a decomposition at the surfaces. All three oxohydroxoferrates are also unstable against the electron beam if the acceleration voltage exceeds about 10 kV, which hampers the EDX analysis (Figure S11, Supporting Information).

2.2. Crystal Structures

The oxohydroxoferrates adopt different orthorhombic structures: **K** crystallizes in space group *Pbca* (Pearson symbol *oP*88) at room temperature and in *Cmce* (*oC*88) above 340(2) K. **Rb** and **Cs** are isostructural to each other but not to **K**, and are always obtained as mixtures of two modifications with space groups *Cmce* (*oC*88′; prime is used to indicate a difference to the high-temperature modification of **K**) and *Immb* (*oI*88). Nonetheless, the structural patterns of these oxohydroxoferrates are very similar. This is also the reason for the choice of
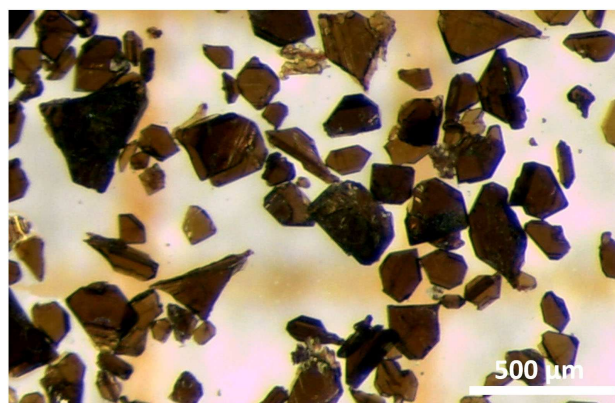
Figure 2. Irregular shaped platelets of **K** obtained from potassium hydroxide hydroflux at q(K) = 1.1.

q(K)	0.4	0.7	1.1	1.4
	α-Fe$_2$O$_3$	K$_{2-x}$[Fe$_4$O$_{7-x}$(OH)$_x$]	K$_2$[Fe$_2$O$_3$(OH)$_2$]	KFeO$_2$

Figure 1. Variety of products within the reaction of iron(III) nitrate and potassium hydroxide depending on the ratio q(K) = n(KOH):n(H$_2$O).

the non-standard setting *Immb* (conventional *Imma*; for crystal structure details see Figure S12, Tables S2 and S3).

All crystal structures consist of folded $_\infty^2[Fe_2O_3(OH)_2]^{2-}$ layers (Figure 3) that host A^+ cations in their trenches and are separated by single-layers of A^+ cations parallel to (010). Every iron(III) cation is coordinated tetrahedrally by three μ-bridging oxide ions and one terminal hydroxide group. Thus, each of the iron-centered tetrahedra shares three of its vertices. Any nodal connectivity of three must create a surface, here a layer. The pronounced folding of these layers, which is stabilized by intramolecular hydrogen bonds of the hydroxide groups, resembles the tertiary structure in proteins, in particular beta pleated sheets. The folding depends on temperature but also on the size of the alkali metal cations (radii for c.n. = 8: K^+: 151 pm, Rb^+: 161 pm, Cs^+: 174 pm).[13] The latter also influences the stacking of the ferrate layers, which then has consequences for the hydrogen bond network as well.

The two-dimensional network of corner-sharing tetrahedra in the oxohydroxoferrates $A_2[Fe_2O_3(OH)_2]$ can be compared with the layered silicates $Li_2Si_2O_5$ and $Rb_2Si_2O_5$ (Figure S13, Supporting Information).[14,15] While the structure of $Li_2Si_2O_5$ differs in the linking of the tetrahedra within the layers (six-membered rings), the structure of $Rb_2Si_2O_5$ has the same net of four- and eight-membered rings as the here presented compounds, yet the folding is much less pronounced, which entails the absence of trenches. Two other related compounds are $H_2Si_2O_5$[16] and $RbHSi_2O_5$,[17] which feature hydrogen bonds between oxohydroxosilicate layers. In these compounds, however, the hydrogen bonds are much shorter, which can be attributed to the much smaller ionic radius of Si^{4+} (26 pm) as compared to Fe^{3+} (49 pm, c.n. = 4).[13]

In the following, the four structure types of the alkali metal oxohydroxoferrates $A_2[Fe_2O_3(OH)_2]$ are discussed in detail. The room temperature modification of **K** (*Pbca*, *oP*88) transforms into the high-temperature modification (*Cmce*, *oC*88) at 340(2) K as DSC experiments as well as a temperature-dependent study of the lattice parameters of a single-crystal consistently show (Figure 4). The jump in the lattice parameters evidences a
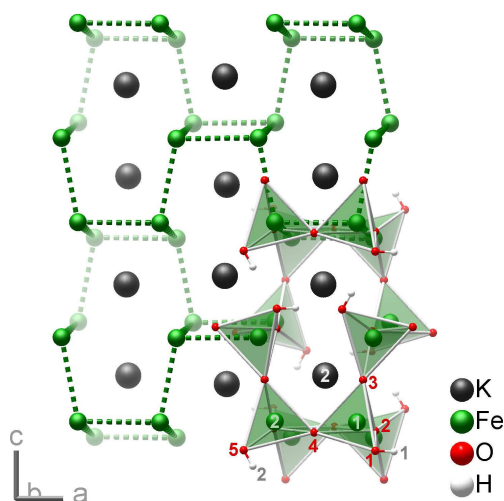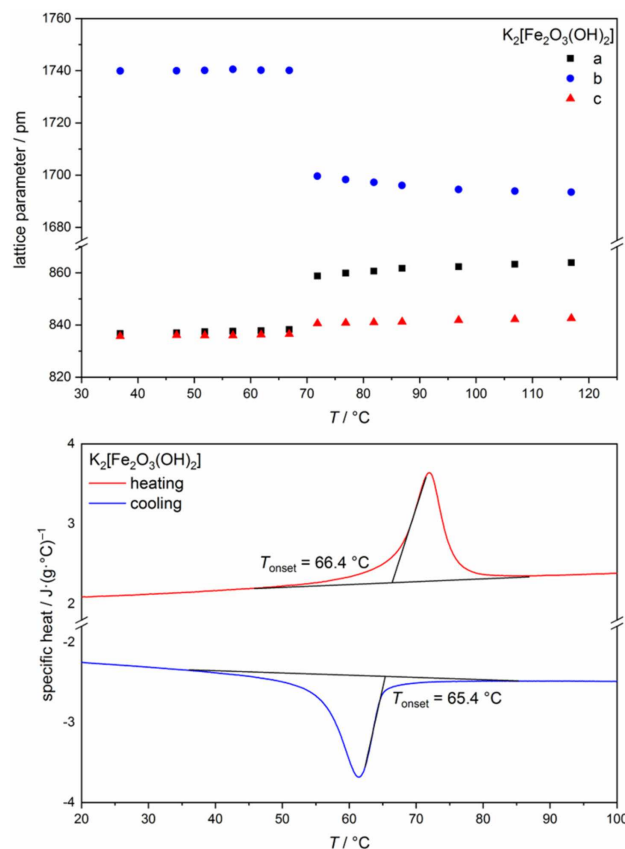

Figure 4. Temperature dependent evolution of lattice parameters, measured on a single-crystal (top; standard derivations are smaller than the symbols) and DSC (bottom) measurement of $K_2[Fe_2O_3(OH)_2]$. The absolute value of the enthalpy is nearly the same for both transitions ($\Delta H \approx 8.7$ J/g).

phase-transition of first order. However, there is no evident hysteresis, and the two modifications are directly linked by a group-subgroup relationship (*klassengleich* of index 2) with only small shifts of the atomic positions. The cell volumes of **K**(*oP*88) at 100 K and **K**(*oC*88) at 370 K differ by $\Delta V/V = +2.5\%$ (Table 1). While a and c elongate by $\Delta a/a = +3.4\%$ and $\Delta c/c = +1.2\%$, the b axis shrinks by $\Delta b/b = -2.2\%$. With respect to the almost unchanged y coordinates of the iron atoms, the widening of the ferrate layer reduces the inter-layer distance proportionally to the thickness of the ferrate layer (by decreasing the Fe–O–Fe angle in the layer center by about 5°).

The disproportionately widening in a is associated with a change in the hydrogen bonding system. The distances O–H···O are 274 and 282 pm at 100 K, but 307 and 290 pm at 370 K

Figure 3. Connectivity in the oxohydroxoferrate layer, shown for **K**(*oP*88).

Table 1. Lattice parameters of $A_2[Fe_2O_3(OH)_2]$ single crystals ($A = $ K, Rb, Cs).

Phase	T/K	a/pm	b/pm	c/pm	V/(10^6 pm³)
K(*oP*88)	100	834.56(6)	1732.8(1)	831.77(6)	1202.8(1)
K(*oC*88)	370	863.42(5)	1695.47(9)	842.22(4)	1232.9(1)
Rb(*oC*88′)	100	912.71(5)	1667.9(1)	850.02(5)	1294.0(1)
Rb(*oI*88)	100	836.29(4)	1701.23(9)	918.61(5)	1306.9(2)
Cs(*oC*88′)	100	945.15(5)	1716.51(9)	870.96(4)	1413.0(1)
Cs(*oI*88)	100	845.83(7)	1742.9(2)	953.31(9)	1405.4(4)
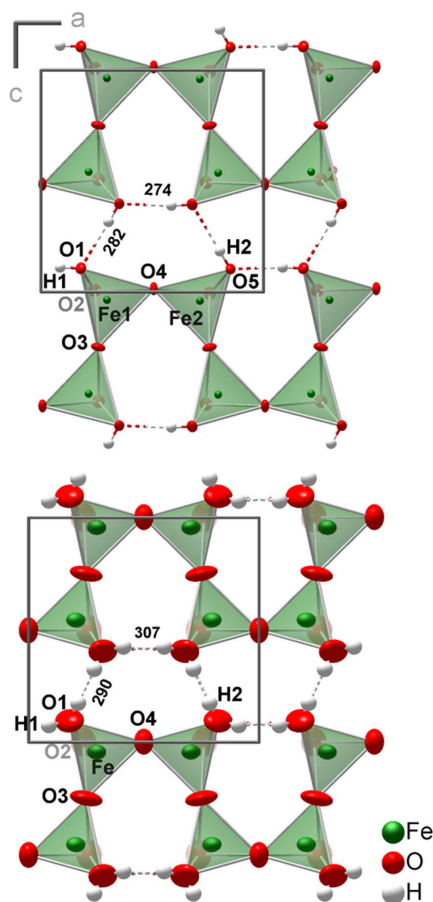
Figure 5. Intra-layer networks of hydrogen bonds in **K**(*oP*88) at 100 K and in **K**(*oC*88) at 370 K. The view is on top of a ferrate layer, of which only the upper half is shown. Ellipsoids represent 90% of the probability density of the atoms (arbitrary size for H). Distances in pm.
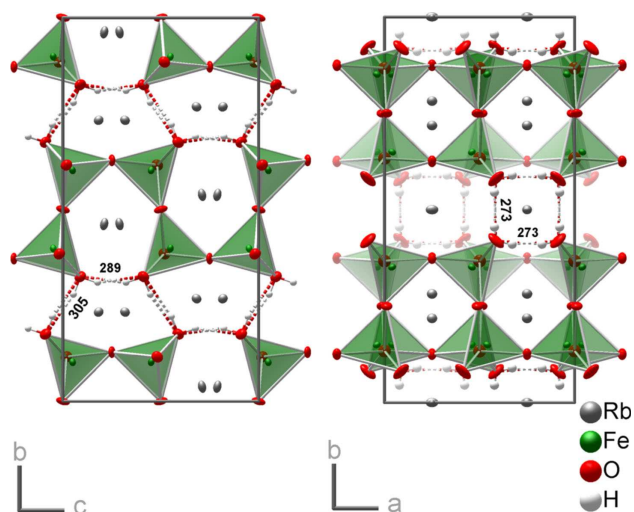
Figure 6. Intra- and inter-layer networks of hydrogen bonds in **Rb**(*oC*88′) and **Rb**(*oI*88). Note the different viewing directions. Ellipsoids enclose 90% of the probability density of the atoms at 100 K (arbitrary size for hydrogen). Distances in pm.

(Figure 5). In the high-temperature form, the mirror plane runs through the center of the hydrogen bond, i.e. the hydrogen atom is in a symmetric double-minimum potential and can be alternately attached to one of the two involved oxygen atoms. As the hydrogen bonds form chains along [100], the actual position of one hydrogen atom will influence all others along [100]. Such a correlated hydrogen shift resembles the Grotthuss mechanism in proton conductors.[18,19] In the room-temperature form **K**(*oP*88), the potential is asymmetric and the hydrogen atom is located at one specific oxygen atom.

The *Cmce* modifications of the rubidium and caesium compounds, **Rb**(*oC*88′) and **Cs**(*oC*88′), have the same layer stacking sequence as **K** but differ in their networks hydrogen bonds. While **K** has only hydrogen bonds within the ferrate layer, **Rb**(*oC*88′) and **Cs**(*oC*88′) have intra- and inter-layer bonds forming chains along [001] (Figure 6, left). This has notable consequences for the lattice parameters. Despite the larger cation, the additional bonding between the layers in **Rb**(*oC*88′) shortens the *b*-axis by −3.8% compared to **K**(*oP*88) (both at 100 K). On the other hand, the loss of bonding along [100] in **Rb**(*oC*88′) elongates the *a*-axis by 9%, which is more than the different sizes of the cations can account for (volume difference 7.3%). As in **K**(*oC*88), the hydrogen atoms are on average disordered (symmetric double-minimum potential) along the chain of hydrogen bond in **Rb**(*oC*88′) and **Cs**(*oC*88′) as well. The distances O−H···O are 289 and 305 pm for the rubidium compound, 300 and 315 pm for the caesium compound.

The *Immb* modifications **Rb**(*oI*88) and **Cs**(*oI*88) differ from the structures discussed before in their stacking sequence of the ferrate layers along [010]. The trenches of neighboring layers are opposing each other according to a mirror plane between them. Again, the hydrogen bonds connect within and between ferrate layers. However, they are not forming chains but square homodromes with O−H···O distances of 273 pm in **Rb**(*oI*88) and 283 pm in **Cs**(*oI*88) (Figure 6, right). Both chiralities of the homodrome are equally probable, in accordance with local *mm*2 symmetry. The hydrogen connectivity is parallel to the (001) plane. Accordingly, the *a*-axes of the *Immb* modifications are much shorter than those of the *Cmce* modifications (−8.6%, −11.1%), while the *c*-axes are much longer (7.7%, 9.0%). The densities of the two modifications are almost equal for each of the compounds, thus it can be argued that they have rather similar lattice energies. This complies with the finding of mixtures of both modifications in all hydroflux syntheses. Moreover, the structure determination of two **Cs**(*oI*88) single-crystals showed some significant residual electron density, which can be explained by stacking faults according to the **Cs**(*oC*88′) structure.

In all compounds, the alkali metal ions are coordinated by 10 oxygen atoms. Significant differences in *A*−O distances and shapes of the coordination polyhedra between the *oC*88′ and *oI*88 modifications can be found (Figure S14 to S16, Supporting Information). The Rb−O distances in the *Cmce* modification of **Rb** (290.2(1) to 360.7(1) pm, average 317.4(1) pm) are longer than in the *Immb* polymorph (279.6(1) to 336.9(1) pm, average 316.6(1) pm). The same holds for **Cs**.

The different hydrogen networks also influence the crystal morphologies: thin plates for *K,* square plates for *Rb* and *Cs* in their *C*-centered modifications, triangular thick bars for their *I*-centered forms.

2.3. Chemical and Thermal Decomposition

Chemical decomposition was studied by exposing crystals of the three oxohydroxoferrates, which were placed on the same SEM sample holder, to air for 1 minute and after the first SEM measurement for another 5 minutes. SEM images of crystals of *K* after the one-minute exposure to air show an overall surface roughening, whereas small parts of crystals of *Rb* and *Cs* show tarnishing (Figure S17 and S18, Supporting Information). After the second air exposure, the SEM images of the decomposition of crystals of all three hydroxoferrates in the 5 min experiment are similar. They show clubs and blisters on the surface, but also long fibers, which have a notably higher alkali metal content.

The thermal stability of the oxohydroxoferrates was characterized by thermogravimetry (TG) and differential thermal analysis (DTA) up to 1000 °C for *K*, to 600 °C for *Rb* and *Cs*, at a heating rate of 5 K min^{-1} under inert conditions in an argon flow. The hydroxoferrates decompose to their anhydrides in the following manner:

$$A_2[Fe_2O_3(OH)_2] \rightarrow 2\,AFeO_2 + H_2O \tag{1}$$
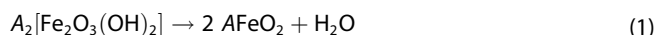
The decomposition temperatures of *Rb* and *Cs* are 343 °C and 348 °C, while *K* dehydrates already at 261 °C (Figure 7, S19 and S20, Supporting Information). The different thermal stabilities can be correlated with the hydrogen bond networks, which are only intra-layer in *K* but inter- and intra-layer in *Rb* and *Cs*. The two modifications of *Rb* and *Cs* seem to have similar thermal stabilities, because only one decomposition signal was found for each of their two-phase mixtures. Small signals in the DTA of *K* at 713 °C and of *Rb* at 447 °C match the
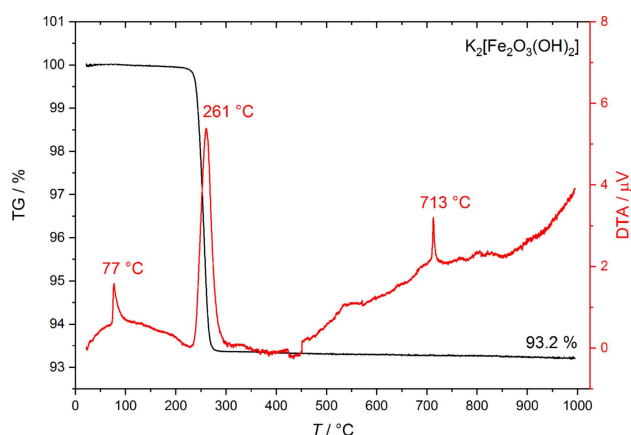
structural phase transitions of $KFeO_2$ and $RbFeO_2$ from *Pbca* to *Fd$\bar{3}$m* at 715 °C and 448 °C, respectively.[1]

2.4. Infrared Spectra

IR spectroscopy was performed to trace the hydrogen bonds in all three oxohydroxoferrates at room temperature (Figure 8). The two different hydrogen bonds in *K* give rise to one very broad valence band with maximum at 3189 cm^{-1}. The spectrum of *Rb* has one broad band at 3136 cm^{-1} with two shoulders at 3315 and 3405 cm^{-1}. The broad band seems to be caused by the hydrogen bonds of the *Cmce* modification, which is structurally related to the one of *K*. The sharper shoulders are probably caused by the *Immb* modification, which lacks an extended hydrogen bonding network. The shorter oxygen distances in the *Immb* modification suggest that these bands have higher wavenumbers than those of the *Cmce* modification. Similarly, *Cs* shows a broad band with maximum at 3272 cm^{-1} and two sharper main bands at 3399 and 3446 cm^{-1} with shoulders at 3351 and 3494 cm^{-1}. The strength of the hydrogen bonds of the alkali metal oxohydroxoferrates is similar to the simplest oxohydroxoferrate β-FeOOH (akaganéite), which has a broad doublet at 3480 cm^{-1} and 3390 cm^{-1}.[20] The energy of vibrations in the IR spectra depends on different factors, the Fe—O and *A*—O bond length and the atomic masses of the metal atoms being crucial factors, so that a qualitative comparison of the hydrogen bond strength between the alkali metal oxohydroxoferrates is not possible.[21]

2.5. Mössbauer Spectra

Although bond-valence sums[22] clearly indicate iron(III) and all hydrogen position could be identified in difference Fourier maps and refined without restraints (except for their occupancies), we measured ^{57}Fe Mössbauer spectra of *K* at room temperature and 6 K to probe independently the iron oxidation state. Both spectra (Figure 9) could be well reproduced with one signal with an isomer shift of $\delta = 0.085(2)$ mm·s^{-1} at 293 K

Figure 7. Thermal analysis of *K* up to 1000 °C with a heating rate of 5 K min^{-1}.
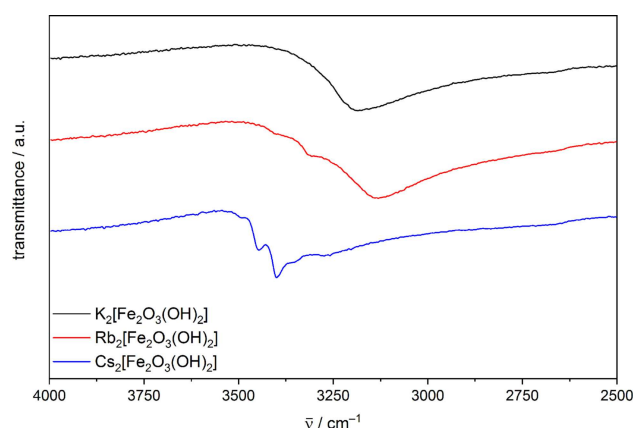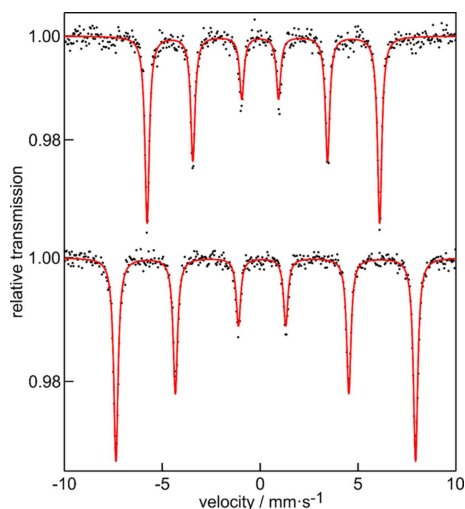

Figure 8. IR spectra showing the valence vibrations of the hydroxide group of the three alkali metal oxohydroxoferrates.

Figure 9. Experimental (data points) and simulated (red line) ^{57}Fe Mössbauer spectra of $K_2[Fe_2O_3(OH)_2]$ measured at room temperature (top) and 6 K (bottom).

and $\delta = 0.194(1)$ mm·s^{-1} at 6 K (Table 2). The small differences in the isomer shifts is a consequence of the second order Doppler shift. The total isomer shift can be described as the sum of the electric monopole interaction and the second order Doppler shift which depends on the mean square of velocity of the nucleus.[23]

The experimental line width was fixed at $\Gamma = 0.27$ mm·s^{-1} during the fitting procedure, which is in the usual range for ^{57}Fe Mössbauer spectra. The small quadrupole shift parameter of $\Delta E_Q = 0.163(3)$ mm·s^{-1} (293 K) and $\Delta E_Q = 0.186(3)$ mm·s^{-1} (6 K) are in accordance with the just slightly distorted tetrahedral environment of the Fe sites.[24] Although the $K(oP88)$ structure contains two crystallographically independent iron sites, these could not be resolved. We just observe the envelope of both sub-signals with very close line width, quadrupole shift and isomer shift. In comparison with Mössbauer spectroscopic data of other iron oxides and hydroxides, the isomer shift is in good agreement with iron(III) in tetrahedral coordination.[25] The 6 K spectrum shows full magnetic hyperfine field splitting with $B_{Hf} = 47.5(1)$ T, similar to $K_{2-x}[Fe_4O_{7-x}(OH)_x]$.[11] For the spectrum at room temperature we observe similar full magnetic hyperfine field splitting but with a reduced hyperfine field of $B_{Hf} = 36.8(1)$ T. The temperature dependence of the hyperfine field usually follows a Brillouin function. Since the hyperfine field at room temperature is still high, the transition to the paramagnetic state is at much higher temperature. The magnetic moment per iron atom at 6 K was derived from the magnetic
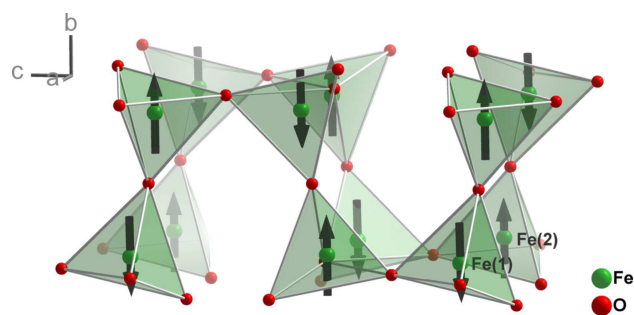
hyperfine field by using the conversion factor of 12.5 T corresponding to 1 μ_B,[26] resulting in a moment of 3.8 μ_B per iron atom, in close agreement with the neutron diffraction data.

2.6. Magnetic Properties and Structure

The fast decomposition of the oxohydroxoferrates impedes the magnetic measurements. Even washing results in a minor amount of amorphous iron oxide, which has a very large magnetic moment in comparison to the oxohydroxoferrates. Therefore, we prepared the samples for magnetic measurements directly out of the vacuum-dried hydroflux for each compound, which means, without removing the alkali metal hydroxides. The amounts of the bases were determined by titration experiments and resulted in approximate oxohydroxoferrate contents between 10 and 20%.

Magnetic measurements of K revealed diamagnetic behavior between 1.8 and 300 K, which are qualitative results only due to the high content of diamagnetic alkali metal hydroxide (Figure S21 Supporting Information). The small increase of the magnetic moment is probably caused by a trace of decomposition product, which could form during the different transfer processes. The measured magnetic moments were corrected by the respective diamagnetic increments, which results in a positive susceptibility.

As the vanishing susceptibility of the iron(III) compound suggest antiferromagnetic coupling, neutron diffraction data were collected for K powder samples at 4 and 300 K (Figure S22 and S23, Table S4 and S5, Supporting Information). The diffraction patterns for both temperatures are nearly identical, confirming the constant magnetic behavior between 1.8 and 300 K seen in magnetization and Mössbauer spectroscopic measurements. Rietveld refinements, including the magnetic scattering intensities, led to a spin structure with the magnetic space group $Pbc'a'$; the propagation vector k equals [000]. The moments of the iron atoms are roughly aligned along [010], i.e. nearly perpendicular to the ferrate layers and antiferromagnetically coupled to their three neighbors via oxygen superexchange (Figure 10). The distributions of the magnetic and nuclear intensities for the measurements at 4 k and 300 k are given in Figures S24 and S25 of the Supporting Information.

Table 2. Fitting parameters of ^{57}Fe Mössbauer spectroscopic measurements of $K(oP88)$ at 293 and 6 K; $\delta =$ isomer shift, $\Delta E_Q =$ electric quadrupole shift, $\Gamma =$ experimental line width, B_{Hf} (T) = hyperfine splitting. Parameters marked with an asterisk were kept fixed during the fitting procedure.

T/K	δ/(mm·s^{-1})	ΔE_Q/(mm·s^{-1})	Γ/(mm·s^{-1})	B_{Hf}/T
293	0.085(2)	0.163(3)	0.27*	36.8(1)
6	0.194(1)	0.186(2)	0.27*	47.5(1)

Figure 10. Magnetic structure of K at 4 K. Black arrows indicating the spin orientation.

Orienting magnetic measurements of *Rb* and *Cs* samples (including RbOH or CsOH) suggest that these $A_2[Fe_2O_3(OH)_2]$ compounds are also antiferromagnets (Figure S26 and S27, Supporting Information). The small moment of the *Rb* sample might be caused by traces of $RbFeO_2$.[27] Neutron scattering experiments of *Rb* or *Cs* were not considered because of the inseparability of the two polymorphs.

3. Conclusions

Hydroflux conditions provide access to oxohydroxoferrates $A_2[Fe_2O_3(OH)_2]$ ($A =$ K, Rb, Cs), in which the base concentration q $(A) = n(AOH):n(H_2O)$ proved to be a crucial synthesis parameter. The compounds are sensitive to moist air and decompose upon heating to their anhydrides $AFeO_2$ and water. All oxohydroxoferrates crystallize in layered orthorhombic structures that are quite similar but differ in the stacking sequences of their $_\infty^2[Fe_2O_3(OH)_2]^{2-}$ layers and especially in their hydrogen bond networks. The latter influence the decomposition temperatures, the structures and the morphology of the crystals. The compounds are antiferromagnets with Néel temperatures above room temperature. As shown for $K_2[Fe_2O_3(OH)_2]$, the magnetic moments of the iron(III) cations are aligned antiparallel in neighboring corner-sharing tetrahedra.

Experimental Section

Synthesis

The alkali metal oxohydroxoferrates(III) $A_2[Fe_2O_3(OH)_2]$ ($A =$ K, Rb, Cs) were synthesized in a hydroflux of the respective alkali metal hydroxide. These reactions were carried out in a PTFE-lined 23 mL Parr type 4749 A autoclave to prevent water loss. In a typical synthesis for $K_2[Fe_2O_3(OH)_2]$ the hydroflux consists of water and KOH (85%, VWR Chemicals) with the molar ratio of 1.0:1.1. For the hydroflux of $RbOH \cdot xH_2O$ (99.8%-Rb, abcr) and $CsOH \cdot H_2O$ (96%, abcr) a lower base quantity (water:hydroxide 1:0.8) was used, whereby no deionized water was added due to the existence of water in the commercial hydroxides and in $Fe(NO_3)_3 \cdot 9H_2O$. 3 mmol of $Fe(NO_3)_3 \cdot 9H_2O$ ($\geq 98\%$, Alfa Aesar) were added to each of the hydroflux mixtures. The autoclave was heated to 200 °C at 2 Kmin^{-1} and kept for 10 h before cooling down to room temperature at the rate of -0.5 Kmin^{-1}. The crystals of the products were isolated by washing with methanol and stored under argon.

Single-Crystal X-Ray Diffraction

Intensity data were collected at 100 and 370 K with a four-circle diffractometer Kappa Apex2 (Bruker) equipped with a CCD-detector using graphite-monochromated Mo-$K\alpha$ radiation ($\lambda = 71.073$ pm). Data were corrected for Lorentz and polarization factors,[28] and multi-scan absorption correction was applied.[29] The structures were solved using ShelXT.[30] Structure refinement against F_o^2 with ShelXL[31] included anisotropic displacement parameters for all non-hydrogen atoms. The hydrogen atoms were refined with fixed distance to their oxygen atom and with coupled isotropic displacement parameter for *Rb* and *Cs*. For *K*, the hydrogen atoms were refined without any restraints.

Tables S2 and S3 of the Supporting Information contain crystal structure data and selected interatomic distances and angles. Further details of the crystal structure determinations are available from the Fachinformationszentrum Karlsruhe, D-76344 Eggenstein-Leopoldshafen (Germany), E-mail: crysdata@fiz-karlsruhe.de, on quoting the depository number CSD-1954741 for $K_2[Fe_2O_3(OH)_2]$ (*Pbca*), CSD-1954740 for $K_2[Fe_2O_3(OH)_2]$ (*Cmce*), CSD-1954743 for $Rb_2[Fe_2O_3(OH)_2]$ (*Cmce*), CSD-1954742 for $Rb_2[Fe_2O_3(OH)_2]$ (*Immb*), CSD-1954739 for $Cs_2[Fe_2O_3(OH)_2]$ (*Cmce*), CSD-1954738 for $Cs_2[Fe_2O_3(OH)_2]$ (*Immb*).

The lattice parameters of a $K_2[Fe_2O_3(OH)_2]$ single-crystal were measured between 270 and 400 K with a Rigaku Oxford Diffraction SuperNova system using Mo-$K\alpha$ radiation ($\lambda = 71.073$ pm) generated by a Nova micro-focus X-ray source.

Powder X-Ray Diffraction

Phase identification and purity were determined on an STADI P (Stoe & Cie.) equipped with a curved Ge-monochromator using Mo-$K\alpha_1$ radiation ($\lambda = 70.932$ pm) and with a Dectris Mythen 1 K detector at room temperature. The program package Topas-Academics v.5 was used for all Rietveld refinements.[32]

Neutron Diffraction

The characterization of the magnetic properties of *K* was carried out on the SPODI high-resolution powder diffractometer at the research reactor Heinz Maier-Leibnitz in Munich (FRM II). Diffraction data were collected at 4 K and 300 K using a closed-cycle cryostat and a Ge(551) monochromator with a neutron wavelength of $\lambda = 154.83$ pm and a step width of 0.05°. The detector bank consists of 80 spatially resolved ^{3}He counter tubes (active measuring height: 300 mm; 2° angular range).[33,34] The refinement of the nuclear and magnetic structure was done with Jana2006.[35] To minimize correlations, the components of the iron moments that were refined to 0 within 3σ were fixed at this value.

IR-Spectroscopy

IR spectra were recorded using a Bruker Vertex 70 FT-IR spectrometer. The device was operated in the ATR mode (diamond), working with a measuring range of 4000 to 600 cm^{-1}. The software used to evaluate the spectra was OPUS 6.5.[36]

Magnetic Measurements

The magnetic properties of $K_2[Fe_2O_3(OH)_2]$ were analyzed with a CRYOGENIC Cryogen Free Measurement System (CFMS). The measured data were recorded using a Vibration Sample Magnetometer (VSM) in the temperature range from 1.8 K to 300 K. The compounds $Rb_2[Fe_2O_3(OH)_2]$ and $Cs_2[Fe_2O_3(OH)_2]$ were analyzed with a SQUID magnetometer MPMS from Quantum Design in VSM mode in the temperature range from 1.8 K to 350 K.

Thermal Analysis

The thermal properties of the hydroxoferrates were characterized by TG and DTA with a Netzsch STA 449 C in an argon-filled glovebox from 25 to 1000 °C with the heating rate of 5 Kmin^{-1}. The phase transition of $K_2[Fe_2O_3(OH)_2]$ was analyzed by DSC with a PerkinElmer DSC 8500 in an argon-filled glovebox from -30 to 140 °C with a heating and cooling rate of ± 5 Kmin^{-1}.

Acknowledgements

Conflict of Interest

The authors declare no conflict of interest.

[1] N. Z. Ali, J. Nuss, D. Sheptyakov, M. Jansen, *J. Solid State Chem.* **2010**, *183*, 752–759.

[2] G. Frisch, C. Röhr, *Z. Naturforsch. B* **2014**, *60*, 732–740.

[3] H.-P. Müller, R. Hoppe, *Z. Anorg. Allg. Chem.* **1990**, *580*.

[4] G. Frisch, C. Röhr, *Z. Naturforsch. B* **2014**, *60*, 1224–1230.

[5] H. Rieck, R. Hoppe, *Angew. Chem.* **1973**, *85*, 589–590; *Angew. Chem. Int. Ed.* **1973**, *12*, 673–674.

[6] D. E. Gheorghe, A. P. Litvinchuk, A. Möller, *Z. Anorg. Allg. Chem.* **2012**, *638*, 2087–2092.

[7] K. Kitahama, R. Kiriyama, *Bull. Chem. Soc. Jpn.* **1976**, *49*, 2748–2754.

[8] P. L. Knöchel, P. J. Keenan, C. Loho, C. Reitz, R. Witte, K. S. Knight, A. J. Wright, H. Hahn, P. R. Slater, O. Clemens, *J. Mater. Chem. A* **2016**, *4*, 3415–3430.

[9] A. M. Latshaw, W. M. Chance, G. Morrison, K. D. zur Loye, B. O. Wilkins, M. D. Smith, P. S. Whitfield, M. J. Kirkham, S. A. Stoian, H.-C. zur Loye, *Angew. Chem. Int. Ed.* **2016**, *55*, 13195–13199; *Angew. Chem.* **2016**, *128*, 13389–13393.

[10] W. M. Chance, D. E. Bugaris, A. S. Sefat, H.-C. zur Loye, *Inorg. Chem.* **2013**, *52*, 11723–11733.

[11] R. Albrecht, J. Hunger, T. Block, R. Pöttgen, A. Senyshyn, T. Doert, M. Ruck, *ChemistryOpen* **2019**, *8*, 74–83.

[12] W. M. Chance, *Hydroflux Synthesis: A New and Effective Technique for Exploratory Crystal Growth*, PhD Thesis, University South Carolina, USA, **2014**.

[13] R. D. Shannon, *Acta Crystallogr. Sect. A* **1976**, *32*, 751–767.

[14] R. I. Smith, R. A. Howie, A. R. West, A. Aragón-Piña, M. E. Villafuerte-Castrejón, *Acta Crystallogr. Sect. C* **1990**, *46*, 363–365.

[15] B. H. W. S. de Jong, P. G. G. Slaats, H. T. J. Supèr, N. Veldman, A. L. Spek, *J. Non-Cryst. Solids* **1994**, *176*, 164–171.

[16] F. Liebau, *Z. Kristallogr. – Cryst. Mater.* **1964**, *120*, 427–449.

[17] I. Bull, J. B. Parise, *Acta Crystallogr. Sect. C* **2003**, *59*, i100–i102.

[18] C. J. T. de Grotthuss, *Ann. Chim.* **1806**, *58*, 54–73.

[19] N. Agmon, *Chem. Phys. Lett.* **1995**, *244*, 456–462.

[20] E. Murad, J. L. Bishop, *Am. Mineral.* **2015**, *85*, 716–721.

[21] C. A. Geiger, G. R. Rossman, *Am. Mineral.* **2018**, *103*, 384–393.

[22] N. E. Brese, M. O'Keeffe, *Acta Crystallogr. Sect. B* **1991**, *47*, 192–197.

[23] D. Barb, *Grundlagen Und Anwendung Der Mößbauer-Spektroskopie*, Akademie-Verlag, Berlin, **1980**.

[24] G. K. Shenoy, F. E. Wagner (Eds.), *Mößbauer Isomer Shifts*, North-Holland Publishing Company, Amsterdam, **1978**.

[25] F. Menil, *J. Phys. Chem. Solids* **1985**, *46*, 763–789.

[26] O. Massenet, H. Daver, V. D. Nguyen, J. P. Rebouillat, *J. Phys. F: Met. Phys.* **1979**, *9*, 1687.

[27] N. Z. Ali, *New Ternary Alkalioxometallates of the First-Row Transition-Metal Elements through the Azide Nitrate Route*, PhD Thesis, Universität Stuttgart, Germany, **2011**.

[28] *APEX2*, Bruker AXS Inc., Madison, Wisconsin, USA, **2014**.

[29] G. M. Sheldrick, *Sadabs: Area-Detector Absorption Correction*, Bruker AXS Inc., Madison, Wisconsin, USA, **2014**.

[30] G. M. Sheldrick, *ShelXT*, Universität Göttingen, Germany, **2014**.

[31] G. M. Sheldrick, *Acta Crystallogr. Sect. A* **2008**, 112–122.

[32] A. Coelho, *Topas-Academic, v. 5*, Brisbane, Australia, **2012**.

[33] M. Hölzel, A. Senyshyn, R. Gilles, H. Boysen, H. Fuess, *Neutron News* **2007**, *18*, 23–26.

[34] M. Hölzel, A. Senyshyn, N. Jünke, H. Boysen, W. Schmahl, H. Fuess, *Nucl. Instrum. Methods Phys. Res. Sect. A* **2012**, *667*, 32–37.

[35] V. Petříček, M. Dušek, L. Palatinus, *Z. Kristallogr. – Cryst. Mater.* **2014**, *229*, 345–352.

[36] *Opus 6.5*, Bruker Optik, **2007**.

[37] G. J. Long, T. E. Cranshaw, G. Longworth, *Mössbauer Eff. Ref. Data J.* **1983**, 42–49.

[38] R. A. Brand, *WinNormos for Igor6, Version for Igor 6.2 or above: 22.02.2017*, Universität Duisburg, Germany, **2017**.